IOP Publishing Superconductor Science and Technology
Supercond. Sci. Technol. **27** (2014) 055013 (6pp) doi:10.1088/0953-2048/27/5/055013

High normal zone propagation velocity in second generation high-temperature superconductor coated conductors with a current flow diverter architecture

Christian Lacroix, Yannick Lapierre, Jonathan Coulombe and Frederic Sirois

Department of Electrical Engineering, Polytechnique Montréal, Montréal, QC, H3C 3A7, Canada

E-mail: christian.lacroix@polymtl.ca

Received 13 November 2013, revised 15 January 2014
Accepted for publication 31 January 2014
Published 20 March 2014

Abstract

A high normal zone propagation velocity (NZPV) is a desirable feature in second generation (2G) high-temperature superconductor (HTS) coated conductors (CCs) in order to reduce the probability of developing destructive hot spots. In this work we investigated experimentally the impact of inserting a highly resistive layer that partially covers the HTS–stabilizer interface of 2G HTS CCs. This new layer was called a 'current flow diverter' (CFD). The purpose of the CFD is to concentrate the current at the edges of the tape when the current transfers from the HTS to the stabilizer upon a quench event. A series of commercial 2G HTS tapes were modified in order to integrate a CFD into them. Measurements realized on these modified tapes showed that the CFD architecture allowed the NZPV to be enhanced by at least two orders of magnitude in comparison with unmodified commercial tapes. Furthermore, it was shown that the NZPV can be significantly enhanced with a very small increase in the HTS–stabilizer interfacial resistance, which is of prime importance for the reliability of current contacts in real applications.

Keywords: quench, coated conductors, hot spots, high-temperature superconductor

(Some figures may appear in colour only in the online journal)

1. Introduction

The very high operating current densities ($>$MA cm^{-2}) of second generation (2G) high-temperature superconductor (HTS) coated conductors (CCs) make them candidates of choice for developing power devices such as superconducting fault current limiters [1], superconducting cables [2], superconducting transformers [3], superconducting electromagnets [4], superconducting motors [5], superconducting magnetic energy storage [6], etc. However, one of the major issues with 2G HTS CCs is that they are prone to develop destructive 'hot spots', particularly when the transport current is close to their critical current (I_c). A hot spot is a thermal instability that propagates along the length of the conductor at a given speed, often called the 'normal zone propagation velocity' (NZPV), in reference to the transition from the superconductor to the normal (i.e. 'non-superconducting') state.

Destructive hot spots in 2G HTS CCs result from a combination of low NZPV [7, 8] and the presence of defects in the microstructure that reduce the local I_c [9, 10]. Since defects cannot be completely eliminated, it seems that unless one increases significantly the thickness of the metallic sheath (often called the 'stabilizer') [11] the only way to reduce the severity of hot spots is to increase the NZPV. One way to do so is to increase the interfacial resistance between the superconducting layer and the stabilizer. Although this approach has been widely studied in the past for low-temperature superconducting wires [12], it is only recently that it has been proposed for increasing the NZPV in 2G HTS CCs [13].

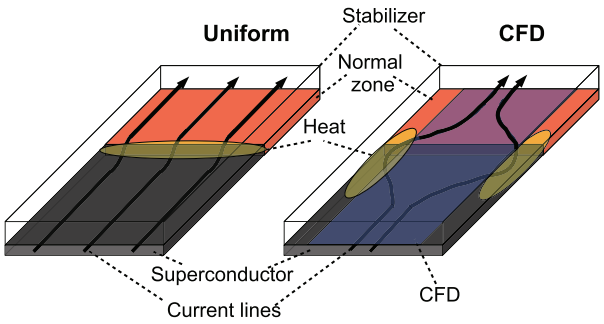

Figure 1. Schematic view of the current path (arrows) in a tape with (i) a uniform interface and (ii) a CFD (blue) interface. The current circumvents the normal zone (red) by transferring from the superconducting layer (gray) to the stabilizing layer (transparent box). The yellow regions indicate where heat is generated, i.e. uniformly across the width (uniform), and along the edges of the tape (CFD).

It was later demonstrated experimentally that the NZPV in 2G HTS CCs can be enhanced by two orders of magnitude when their interfacial resistance (R_i) is increased by three orders of magnitude in comparison with commercial tapes [14]. However, such high values of R_i significantly increase the heat generated at the current contacts, which makes the tape very likely to quench at any physical connection with a normal conductor. This, of course, is unacceptable from a practical point of view.

2. Current flow diverter tape architecture

In order to achieve high NZPVs while keeping R_i at reasonably low values, we propose the introduction of a highly resistive layer between the superconductor and the stabilizer, which only partially covers the interface (the resistance of the remaining interface regions remains low) [15]. The purpose of this architecture is to force the current to follow a specific path when the current transfers from the HTS to the stabilizer, resulting in the localized generation of heat that partially quenches the cross section of the HTS tape. For this reason we use the term *current flow diverter* (CFD) to name this new 2G HTS CC architecture.

For the architecture investigated in this work, a CFD was inserted at the center of the tape, as shown in figure 1, in comparison with a 'uniform' architecture (classical approach). In the uniform architecture case the current is uniformly distributed along the width of the tape when it transfers from the superconducting layer to the stabilizer. With the CFD architecture, when a normal zone appears, the current is forced to flow around the CFD, passing solely by the edges of the tape (where R_i is very low). All heat is therefore generated at the edges of the tape, which considerably changes the quench dynamics, as shown below.

In this work, we present experimental results obtained on 2G HTS CCs in which a CFD had been inserted. First, we provide details about sample fabrication and characterization. Then, experimental data for R_i and NZPV obtained on CFD tapes are presented, analyzed and compared with data obtained on uniform tapes. Finally, we discuss the physical phenomena that drive the quench dynamics in CFD tapes.

3. Experimental procedure

3.1. Preparation of samples

Experiments were carried out on 4-mm-wide 2G HTS CCs ($I_c = 102$ A at 77 K) purchased from SuperPower Inc. The thicknesses of the substrate (Hastelloy®), buffer layers ($Al_2O_3/Y_2O_3/MgO/LaMnO_3$) and HTS layer (REBaCuO, where RE stands for rare earth) were 50, 0.15 and 1 μm, respectively. A silver envelope was used as the stabilizer: this had a thickness of $\approx$1.2 μm on top of the HTS layer and $\approx$1 μm on the edges of the tape and on the substrate side.

Using the following procedure, we could successfully integrate a CFD at the HTS–stabilizer interface of commercial 2G HTS CCs. First, we removed the silver from the location where we wanted to insert the CFD with the help of chemical etching. A solution consisting of 25 vol.%H_2O_2:25 vol.% NH_4OH:50 vol.%H_2O was used to etch the silver at the desired location [16]. A shadow mask was used to protect the silver on the remaining surfaces. The samples were then exposed to air for 24 h at room temperature ($\approx$20 °C) and humidity ($\approx$30–50%). As a side effect of the chemical etching and subsequent exposure to air, a weakly conductive layer was formed at the surface of the REBaCuO layer and was then used as the CFD. The presence of this weakly conductive layer is supported by x-ray photoelectron spectrometry (XPS) and electrical measurements, as presented below. Finally, a silver layer (of thickness 1.4 μm) was deposited on the tape (HTS side) using magnetron sputtering.

A series of short (5 cm) and long (13 cm) samples with CFD widths varying from 2 to 4 mm were fabricated in this way. Critical current measurements realized on the modified tapes showed no degradation of their I_c at liquid nitrogen temperature.

3.2. X-ray photoelectron spectrometry

XPS analysis was performed on a VG Scientific ESCALAB MKII with a Mg Kα source (300 W). The charge correction factor used was the difference between the value of 285.0 eV and the binding energy of C 1s. Background extraction was performed with the Shirley method. Argon ion milling (1 kV) was used to perform depth profiling of the REBaCuO surface. Based on the expected average milling rate of the elements included in REBaCuO and the milling rate of Al as measured with our setup, we roughly estimate the milling rate of REBaCuO to be $\approx$2 nm min^{-1}.

3.3. Measurement of interfacial resistance

The interfacial resistance (R_i) was measured at liquid nitrogen temperature using a four-point resistance method, as described in [14]. In reality, the method described in that reference allows the joint resistance (R_j) to be measured between the two halves of a short sample that were soldered face-to-face (HTS sides together) using an In97%–Ag3% alloy. During soldering, the temperature was kept low ($\approx$160 °C) to avoid modifying the properties of the HTS–Ag interface [17]. The soldered area was $\approx$0.2 cm^2. In addition, in order to make sure the current

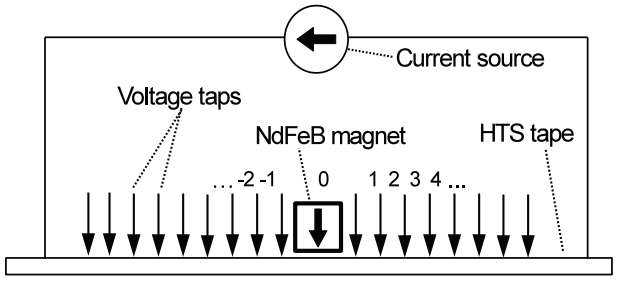

Figure 2. Schematic of the setup used to measure the NZPV. Voltage probes were numbered by pairs relative to the location of the magnet (between pair #0).

was passing through the modified interface, the silver next to the soldered area was etched (see figure 2 in [14] for a detailed schematic).

In order to extract R_i from the R_j measurements, one must carefully interpret the results. Indeed, R_j consists of the sum of several resistances in series, which in our case can be expressed as

$$R_j(f) = 2R_i(f) + 2R_{Ag} + R_s, \quad (1)$$

where R_i is the interfacial resistance between the REBaCuO and Ag layers, R_{Ag} is the resistance of the Ag layers, R_s is the resistance of the solder and f is the CFD coverage fraction (CFD width divided by the total width of tape). We note that while R_{Ag} can be neglected, R_i and R_s can be of the same order ($\approx$1–100 nΩ cm^{-2}) [18], limiting the measurement accuracy on R_i when it has a very low value. However, we can find an estimation of the interfacial resistance, namely $\tilde{R}_i$, which can be expressed as

$$\tilde{R}_i(f) \approx R_j(f)/2 \approx R_i(f) + R_s/2. \quad (2)$$

Note that when $R_i(f) \gg R_s$, we obtain $\tilde{R}_i(f) \approx R_j(f)/2 \approx R_i(f)$, which is the approximation we used throughout this paper. It should also be emphasized that R_i depends on f, whereas R_s is roughly a constant for all samples measured, providing a means to remove its contribution from the measurements at very low R_i values if required.

3.4. Measurement of NZPV

Figure 2 presents a schematic view of the setup that was used to measure the NZPV of the samples prepared above. This setup is similar to that used in [14], except for the current source. The current source used in this work was built specifically for measuring high NZPVs at constant current. More specifically, this source generates square current pulses between 0 and 140 A, for durations of 1–20 ms (for example, see inset in figure 5). A fast feedback control, based on the design described in [19], allows a constant current to be maintained at all times, even when the tape exhibits a very fast increase of resistance, which happens every time a high NZPV tape quenches.

A cylindrical NdFeB magnet (diameter 3 mm) was used to initiate the quench at the desired location. The strong magnetic field generated by the magnet is sufficient to locally reduce I_c and simulate a defect in the HTS layer, as in [8, 14]. A series of equally spaced voltage probes were used to record the voltage over time at various locations along the tape (the distance between two successive probes being $\approx$2.5 mm). The probes were numbered by pairs in a sequential way (positive on the right, negative on the left) with respect to the magnet location (pair #0). Each pair of probes provided a differential measurement from which we could extract an average electric field, as shown in the next section.

Finally, all NZPV measurements performed in this experiment were carried out at 77 K in a liquid nitrogen bath.

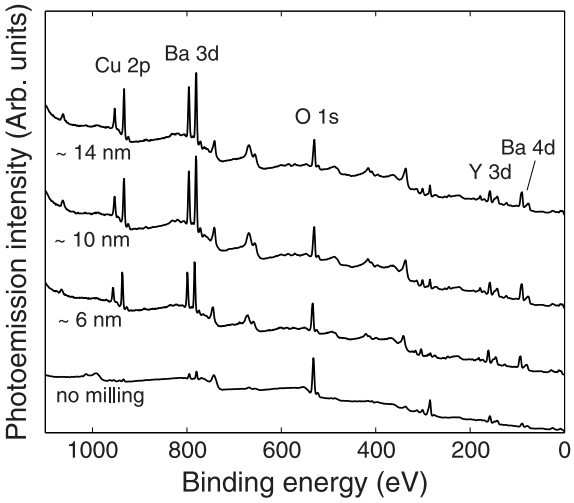

Figure 3. Results of XPS measurements realized on the HTS side of a sample whose silver stabilizer was etched and then exposed to ambient air for 24 h. Measurements were performed at different depths after successive milling steps which lasted 3 min ($\approx$6 nm deep), 3 + 2 min ($\approx$10 nm deep) and 3 + 2 + 2 min ($\approx$14 nm deep).

4. Results and discussion

In order to characterize the CFD, XPS measurements were performed on the HTS side of a sample whose silver was etched and then exposed to ambient air for 24 h. Using argon ion milling, it was possible to perform the XPS characterization at different depths from the REBaCuO surface. Successive milling steps which lasted 3 min ($\approx$6 nm deep), 3 + 2 min ($\approx$10 nm deep) and 3 + 2 + 2 min ($\approx$14 nm deep) were realized.

We can observe from figure 3 that almost no Cu and only a small amount of Ba could be detected at the sample surface (i.e. the top of the CFD) before milling. For the spectra obtained after milling, the main elements detected were Cu, Ba, O and Y, as expected, and almost no difference can be seen between spectra obtained at a depth of 6 nm or more from the surface. The spectrum obtained before milling is thus very different from the spectra obtained after milling. This suggests that the silver etching procedure followed by air exposure that we used above results in a very thin degraded (or contaminated) layer whose thickness is less than $\approx$6 nm. Surface degradation of REBaCuO due to air exposure was already demonstrated in [20], but the degraded (or contaminated) layer observed here from XPS measurements does not necessarily originate

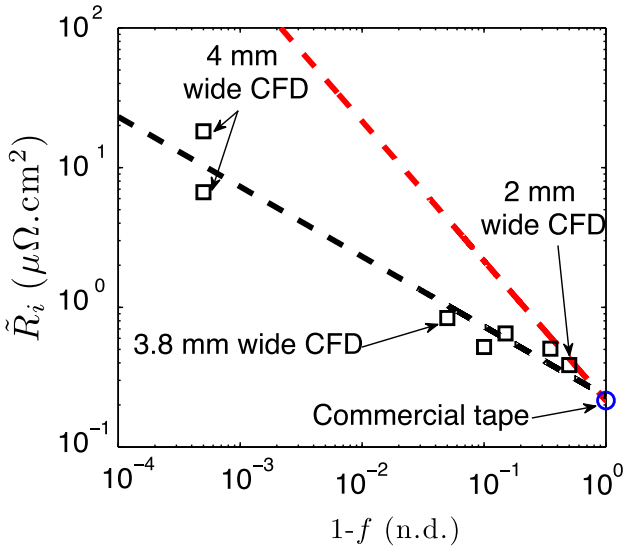

Figure 4. Dependence of $\tilde{R}_\mathrm{i}$ on $1-f$ (black squares), where f is the CFD coverage fraction (CFD width divided by total width of tape) measured at liquid nitrogen temperature. The black dashed line is a fit of the experimental data, showing that $\tilde{R}_\mathrm{i} \propto (1-f)^{-1/2}$. The red dashed line indicates the ideal case (perfectly insulating CFD and $R_\mathrm{i} \gg R_\mathrm{s}$), which corresponds to $\tilde{R}_\mathrm{i} \propto (1-f)^{-1}$.

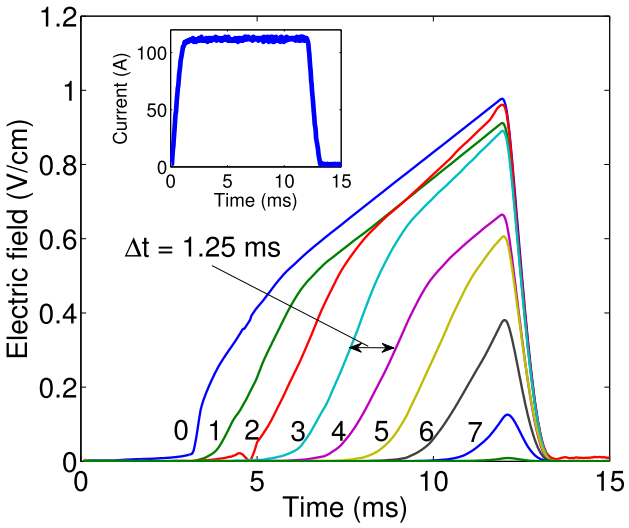

Figure 5. Electric field over time measured from several voltage probes on a sample in which a 3-mm-wide CFD was inserted ($f = 0.75$, $\tilde{R}_\mathrm{i} = 0.5$ $\mu\Omega$ cm^2). The numbers correspond to the pairs of probes as described in figure 2. During measurement, the sample was placed in a liquid nitrogen bath. Inset: applied current versus time.

from the same phenomenon, although it is likely that a similar process is involved.

The dependence of the estimated interface resistance $\tilde{R}_\mathrm{i}$ on $1-f$ at liquid nitrogen temperature is presented in figure 4. As expected, we observe that $\tilde{R}_\mathrm{i}$ increases with the CFD width (i.e. as $1-f$ decreases). This result confirms that our fabrication process creates a resistive layer at the etched surface. Also, the assumption $R_\mathrm{i} \gg R_\mathrm{s}$ seems valid here since if it was not the case, $\tilde{R}_\mathrm{i}$ would be independent of $1-f$ when $1-f$ is close to 1. The measured values are below 1 $\mu\Omega$ cm^2 for all samples, except when the CFD is 4-mm-wide, in which case $\tilde{R}_\mathrm{i} \approx 10$ $\mu\Omega$ cm^2. In that case, the CFD covers all the top surface of the HTS layer, and the regions that are not covered by the CFD are located on the sides of the HTS layer. Since the HTS layer is 1 μm thick, these uncovered regions are very small, which explains why $\tilde{R}_\mathrm{i}$ is much higher compared to the other samples.

It is worth noting that with a perfectly insulating CFD, the interfacial resistance R_i should scale with $(1-f)^{-1}$, i.e. $R_\mathrm{i} = R_0(1-f)^{-1}$, where R_0 is the intrinsic interfacial resistance between the superconductor and the stabilizer. For commercial tapes, where $f = 0$, a value of $R_0 \approx \tilde{R}_\mathrm{i}(0) = 0.22$ $\mu\Omega$ cm^2 was measured (blue circle in figure 4). Using this value as a starting point, the ideal characteristics of a CFD tape could be traced (red dashed curve in figure 4).

In comparison with this ideal case, we observe that the experimental data points (black squares) are rather best fitted with a relationship like $\tilde{R}_\mathrm{i} = R_0(1-f)^{-1/2}$ (black dashed curve) instead of being proportional to $(1-f)^{-1}$. This suggests that the CFD might not be sufficiently insulating to completely block the passage of the current and, as a consequence, the current would partially flow through the CFD, especially when the CFD coverage fraction f is high.

An example of NZPV measurement is presented in figure 5. This measurement was obtained on a tape with a 3-mm-wide CFD ($f = 0.75$, $\tilde{R}_\mathrm{i} = 0.5$ $\mu\Omega$ cm^2) in which we imposed a square current pulse of 112 A (see inset). For the sake of clarity, we only show the voltages measured on the right side of the magnet (the pairs of probes with positive numbers in figure 2). We observe that the voltage first appears between pair #0, then #1, #2, etc. The variation of the measured voltage over time is similar for all pairs of probes, except that each curve is shifted in time with respect to the others. The voltage first slowly rises, then increases exponentially up to an electric field value of ≈0.5–0.7 V cm^{-1}, at which point the HTS resistance is in the same range as that of the stabilizer. Beyond this point, we observe a clear change of slope, which physically corresponds to a complete quench of the HTS volume between the voltage taps, as well as heating of the stabilizer, since all current now flows into it (the HTS layer is now very resistive). In other words, this change of regime indicates that the HTS temperature has just risen above its critical temperature (T_c).

By taking the distance between the middle points of two adjacent voltage probes (≈2.5 mm) divided by the time elapsed for reaching the same value of electric field on two successive curves, we finally obtain the NZPV. For instance, in figure 5 we obtain a NZPV of ≈2 m s^{-1}.

The dependence of the NZPV on $\tilde{R}_\mathrm{i}$ for tapes with a CFD interface is presented in figure 6 (black squares). Values of NZPV as high as 16 m s^{-1} were measured, which is ≈35 times higher than those measured on a commercial tape (blue circle). In comparison, tapes with a uniform interface (red diamonds) also yielded NZPV values as high as 16 m s^{-1}, but at a much higher $\tilde{R}_\mathrm{i}$ value (more than 200 $\mu\Omega$ cm^2) [14]. In that latter case, the fabrication method used was different from the one used in this work: the interfacial resistance was modified by first totally removing the silver with chemical

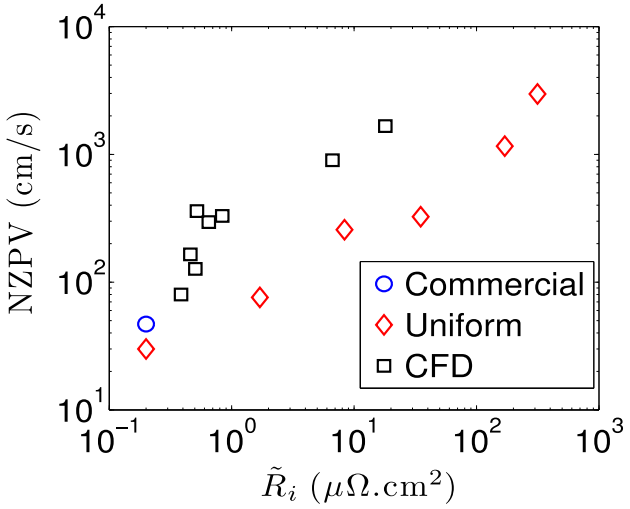

Figure 6. Comparison of the dependence of the NZPV on $\tilde{R}_i$ measured on samples with uniform [14] and CFD architectures (red diamonds and black squares, respectively). The NZPV obtained on a commercial tape is also indicated as a reference (blue circle).

etching (the same recipe as described earlier), followed by the deposition of a silver layer using magnetron sputtering and then thermal annealing in an oxygen atmosphere which lasted approximately 60 min at a temperature between 250 and 350 °C depending on the desired interfacial resistance. It is worth noting that, for the same $\tilde{R}_i$, the NZPV of tapes with a CFD interface is much faster than that of tapes with a uniform interface (up to seven times faster). This behavior holds over the whole range of $\tilde{R}_i$.

A physical explanation to the enhancement of the NZPV with R_i can be formulated by recalling that the NZPV is proportional to the longest of the two following characteristic lengths, namely l_c, the thermal diffusion length (TDL), and the current transfer length (CTL) [13]. When R_i is low, the distance l_c is dominated by the TDL, which is independent of R_i, while at high R_i, l_c is dominated by the CTL, which strongly depends on R_i. The bigger the CTL, the faster the NZPV will be, since the heat associated with a quench is generated over a longer distance in front of the superconducting–normal interface.

The dependence of the NZPV on $\tilde{R}_i$ observed in figure 6 indicates that the high NZPV observed in our CFD samples originates from the presence of a CTL that is larger than the TDL. Also, we deduce that the NZPV measured in the CFD samples is much faster than those with a uniform interface for the same R_i, suggesting that the CFD induces a three-dimensional geometrical effect which forces the current to follow a specific path that further increases the CTL. This conclusion is also supported by finite element calculations [15]. Our architecture therefore opens up a new degree of freedom that can be used to control quench dynamics, i.e. by using tape geometry as a parameter to adjust the CTL and NZPV in 2G HTS CCs, in addition to the interfacial resistance itself.

As a final observation on CFD tapes, we see that the increase in NZPV with $\tilde{R}_i$ is high at low $\tilde{R}_i$ (it reaches a NZPV of $\approx$3 m s^{-1} when $\tilde{R}_i \approx 0.6$ $\mu\Omega$ cm^2), and then it becomes less important. We interpret this behavior as being the result of how we fabricated the CFD samples investigated in this work (with a very thin degraded or contaminated layer as the CFD). As discussed above, it is possible that part of the current flows through the CFD and becomes more and more important as the CFD coverage fraction gets higher. If this is the case, we expect that using a truly insulating CFD would allow an extension of the initial slope over a wider range of $\tilde{R}_i$, as predicted from finite elements calculations [15].

5. Conclusion

In this work, we investigated experimentally the concept of a 'current flow diverter' (CFD) that we developed in order to enhance the NZPV in 2G HTS CCs. Measurements realized on modified commercial 2G HTS CCs, in which a CFD was inserted at the HTS–stabilizer interface, indicated that the CFD allows the NZPV to be increased by several times while keeping the interfacial resistance to acceptable values, as opposed to the uniform interfacial resistance concept previously suggested in the literature. Our results suggest that the enhancement of the NZPV originates from a longer CTL induced by the CFD, which we explain as being the consequence of a three-dimensional geometrical effect which forces the current to follow a specific path. Our work shows that the CFD concept is a promising architecture to reduce the probability of developing destructive hot spots in 2G HTS CCs upon quench events, which is a crucial issue for the commercial success of applications based on 2G HTS CCs. The CFD architecture proposed in this work is relatively simple and should not raise any major issue for future implementation in the actual fabrication processes of 2G HTS CCs.

Acknowledgments

The authors would like to thank the reviewers for their valuable comments and suggestions to improve the quality of the paper. The authors also thank M R Wertheimer, B Dutoit and J Lefebvre for useful discussions, as well as J-H Fournier-Lupien, K McMeekin and N Veerabadren for their technical assistance. This work was supported by research grants from NSERC (Canada) and FRQNT (Québec).

References

[1] Hobl A, Goldacker W, Dutoit B, Martini L, Petermann A and Tixador P 2013 Design and production of the ECCOFLOW resistive fault current limiter *IEEE Trans. Appl. Supercond.* **23** 5601804

[2] Maruyama O *et al* 2013 Development of 66 kV and 275 kV class REBCO HTS power cables *IEEE Trans. Appl. Supercond.* **23** 5401405

[3] Glasson N D, Staines M P, Jiang Z and Allpress N S 2013 Verification testing for a 1 MVA 3-phase demonstration transformer using 2G-HTS Roebel cable *IEEE Trans. Appl. Supercond.* **23** 5500206

[4] Markiewicz W D *et al* 2012 Design of a superconducting 32 T magnet with REBCO high field coils *IEEE Trans. Appl. Supercond.* **22** 4300704

[5] Nick W, Grundmann J and Frauenhofer J 2012 Test results from Siemens low-speed, high-torque HTS machine and description of further steps towards commercialisation of HTS machines *Physica* C **482** 105

[6] Ueda H, Ishiyama A, Muromachi K, Suzuki T, Shikimachi K, Hirano N and Nagaya S 2012 Quench detection and protection of cryocooler-cooled YBCO pancake coil for SMES *IEEE Trans. Appl. Supercond.* **22** 4702804

[7] Wang X, Trociewitz U P and Schwartz J 2007 Near-adiabatic quench experiments on short $YBa_2Cu_3O_{7-\delta}$ coated conductors *J. Appl. Phys.* **101** 053904

[8] Roy F, Dutoit B and Sirois F 2010 Quench nucleation obtained by local reduction of I_c in coated conductors *J. Phys.: Conf. Ser.* **234** 032050

[9] Gurevich A 2001 Thermal instability near planar defects in superconductors *Appl. Phys. Lett.* **78** 1891

[10] Inoue M, Abiru K, Honda Y, Kiss T, Iijima Y, Kakimoto K, Saitoh T, Nakao K and Shiohara Y 2009 Observation of current distribution in high-T_c superconducting tape using scanning Hall probe microscope *IEEE Trans. Appl. Supercond.* **19** 2847

[11] Fu Y, Tsukamoto O and Furuse M 2003 Copper stabilization of YBCO coated conductor for quench protection *IEEE Trans. Appl. Supercond.* **13** 1780

[12] Gurevich A V and Mints R G 1987 Self-heating in normal metals and superconductors *Rev. Mod. Phys.* **59** 941 and references therein

[13] Levin G A, Novak K A and Barnes P N 2010 The effects of superconductor-stabilizer interfacial resistance on the quench of a current-carrying coated conductor *Supercond. Sci. Technol.* **23** 014021

[14] Lacroix C, Fournier-Lupien J-H, McMeekin K and Sirois F 2013 Normal zone propagation velocity in 2G HTS coated conductor with high interfacial resistance *IEEE Trans. Appl. Supercond.* **23** 4701605

[15] Lacroix C and Sirois F 2014 Concept of current flow diverter for accelerating the normal zone propagation velocity in 2G HTS coated conductors *Supercond. Sci. Technol.* **27** 035003

[16] Mbaruku A L and Schwartz J 2008 Fatigue behavior of Y-Ba-Cu-O/Hastelloy-C coated conductor at 77 k *IEEE Trans. Appl. Supercond.* **18** 1743–52

[17] Polak M, Barnes P N and Levin G A 2006 YBCO/Ag boundary resistivity in YBCO tapes with metallic substrates *Supercond. Sci. Technol.* **19** 817

[18] Kato-Yoshioka J, Sakai N, Tajima S, Miyata S, Watanabe T, Yamada Y, Chikumoto N, Nakao K, Izumi T and Shiohara Y 2006 Low resistance joint of the YBCO coated conductor *J. Phys.: Conf. Ser.* **43** 166

[19] Sirois F, Coulombe J, Roy F and Dutoit B 2010 Characterization of the electrical resistance of high temperature superconductor coated conductors at high currents using ultra-fast regulated current pulses *Supercond. Sci. Technol.* **23** 034018

[20] Russek S E, Sanders S C, Roshko A and Ekin J W 1994 Surface degradation of superconducting $YBa_2Cu_3O_{7-\delta}$ thin films *Appl. Phys. Lett.* **64** 3649